JCTC Journal of Chemical Theory and Computation

Relativistic Zeroth-Order Regular Approximation Combined with Nonhybrid and Hybrid Density Functional Theory: Performance for NMR Indirect Nuclear Spin−Spin Coupling in Heavy Metal Compounds

Salvador Moncho

Departament de Química, Universitat Autonoma de Barcelona, 08193 Cerdanyola del Vallés, Spain

Jochen Autschbach*

Department of Chemistry, State University of New York at Buffalo, Buffalo, New York 14260-3000

Received July 27, 2009

Abstract: A benchmark study for relativistic density functional calculations of NMR spin−spin coupling constants has been performed. The test set contained 47 complexes with heavy metal atoms (W, Pt, Hg, Tl, Pb) with a total of 88 coupling constants involving one or two heavy metal atoms. One-, two-, three-, and four-bond spin−spin couplings have been computed at different levels of theory (nonhybrid vs hybrid DFT, scalar vs two-component relativistic). The computational model was based on geometries fully optimized at the BP/TZP scalar relativistic zeroth-order regular approximation (ZORA) and the conductor-like screening model (COSMO) to include solvent effects. The NMR computations also employed the continuum solvent model. Computations in the gas phase were performed in order to assess the importance of the solvation model. The relative median deviations between various computational models and experiment were found to range between 13% and 21%, with the highest-level computational model (hybrid density functional computations including scalar plus spin−orbit relativistic effects, the COSMO solvent model, and a Gaussian finite-nucleus model) performing best.

I. Introduction

Indirect nuclear spin−spin coupling (*J* coupling) is one of the most important nuclear magnetic resonance (NMR) observables. Because of its high sensitivity, the possibility of routine measurements, and its ability to provide useful data about the geometric as well as the electronic structure of chemical compounds, NMR is a widely used technique in chemistry and neighboring scientific disciplines. Consequently, calculations of NMR parameters based on first-principles theory are of high importance to help with the interpretation of experimental data and make predictions. Also, the computation of NMR parameters such as nuclear magnetic shielding and *J* coupling offers new ways of analysis that can enhance the knowledge about NMR observables and improve our ability to understand the implications of experimental NMR data.[1−6]

On the theoretical side, apart from the evidently important topic of modeling NMR parameters, there are few molecular properties that are as sensitive to relativistic effects as *J* coupling: relativistic "corrections" exceeding 100% of the nonrelativistic result are rather common when elements from the sixth row of the periodic table are involved.[6] Moreover, indirect nuclear spin−spin coupling is quite sensitive to approximations used to describe the electron−electron interactions, the quality of the basis set, and just about every other approximation made in the computational model. *J* coupling is therefore an excellent testing ground for elec-

* To whom correspondence should be addressed. E-mail: jochena@buffalo.edu.

10.1021/ct900535d
Published on Web 12/14/2009

tronic structure methods, for relativistic quantum chemical methods, and for relativity−correlation, relativity−solvation, etc., "cross terms".

J couplings with heavy atoms can be challenging to obtain experimentally and reproduce computationally. The reliable calculation of coupling constants for heavy nuclei has some important theoretical requirements for the computational model, most importantly the inclusion of relativistic effects and electron correlation, basis sets that are capable of describing the large relativistic effects on *J* coupling, but also more 'exotic' features such as an adequate finite nuclei representation. Due to the variational instability of the perturbation operators it is also advantageous if the calculation makes use of analytical derivatives techniques instead of a finite-field differentiation.[78]

In recent years, first-principles codes for heavy atom spin−spin coupling constants have become available that consider most, if not all, of these aspects.[7−13] Relativistic effects were considered in these approaches in different ways, making use of four-component theory[7] and various approximate two-component methods (or their scalar relativistic versions) such as the zeroth-order[8,9,12,13] and infinite-order[10] regular approximations (ZORA, IORA), or Douglas−Kroll transformations.[11] Density functional theory (DFT) is usually the method of choice in calculations of heavy nuclei NMR properties in larger metal complexes because it includes electronic correlation at an affordable computational cost. In the past, relativistic NMR computations were a highly specialized research topic. In recent years a substantial body of computational data has become available, demonstrating that in particular relativistic DFT computations of heavy nucleus NMR parameters can be successfully undertaken even for large metal complexes. For a recent overview of theoretical methods and available case studies, see ref 6.

The availability of easy-to-apply relativistic NMR methods of affordable computational cost allows researchers who are not specialized in theory developments to routinely augment their work by first-principles calculations. As a consequence, it is very important to develop protocols for such computations with reasonably well-known and well-understood error bars, perhaps similar in spirit to the established model thermochemistries. It is the intent here to study of performance of a family of computational models for relativistic *J*-coupling computations and determine the error bars with respect to a substantial set of experimental data for coupling constants involving one or two heavy metals. In this way, adequate settings may be determined for an overall agreement of computed spin−spin coupling constants with experiment which allow for an estimation of the error bars of newly computed coupling constants or to gauge whether agreement with experiment has been obtained for 'good enough reasons'. For an assessment of the overall performance of the method a wide range of different couplings needs to be tested, including compounds with different heavy metals and spin−spin couplings through one, two, or more bonds. Having well-tested basis sets available for such computations is also extremely important.

A comparatively widely applied method for relativistic *J*-coupling computations is presently the analytic-derivative ZORA relativistic approach described in refs 8, 9, 12, and13 which includes scalar and spin−orbit relativistic effects, a finite nucleus model, and allows for nonhybrid as well as hybrid DFT computations. The program also includes several methods for chemically motivated analyses of the results.[14−17] A modest number of benchmark data (23 one-bond coupling constants) has been reported along with the original nonhybrid DFT scalar relativistic point-nucleus implementation,[8] indicating overall reasonable agreement with experiment. In this and other previous works, a mix of experimental structures and geometries optimized at various levels of theory have been used along with varying approximations in the exchange-correlation (XC) potential and the XC response kernel. Subsequent applications also have employed varying basis sets, geometries, and functionals. Combining the results from these previous studies into one data set would provide an inconsistent assessment of the method overall.

In this work, we will provide systematic data for 88 one-, two-, and multibond coupling constants involving heavy metal atoms based on a well-defined computational model that is easy to establish in routine computations (see computational details for references): All geometries were optimized at the scalar-ZORA/BP/TZP level of theory with inclusion of a continuum solvation model followed by *J*-coupling computations with a finite nucleus model, the continuum solvation model, and a basis set suitable for *J* coupling. Herein, scalar vs spin−orbit ZORA and nonhybrid vs a hybrid functional (PBE vs PBE0) computations will be compared with experimental data to determine the performance of each computational model with respect to reproducing experimental data. In addition to compiling data for benchmark systems from previous studies, a sizable number of new coupling constants were added and are computed here for the first time. Further, many coupling constants of previously studied systems are computed here for the first time at the hybrid DFT level of theory and including finite nucleus effects. The benchmark set contains 30 two-bond as well as several multibond couplings, a test set large enough to critically assess the performance of relativistic DFT methods using standard functionals to calculate coupling constants with heavy elements other than one-bond couplings.

The approximations leading to deviations between theory and experiment, defining the error bars for each method, are not only in the basis set and functional but also in the overall computational model since most of the experimental *J* couplings were determined in solution at finite temperature. Previous work from our group has highlighted the importance of solvent effects for *J* coupling in metal complexes[6,14,18−22] for which nonhybrid DFT computations have indicated that the use of a continuum model is not always sufficient. In the present benchmark study, errors from a lack of treating explicit solvation dynamically, which would be the most desirable computational model but also a very expensive one, will therefore contribute to the error bars of each computational model. Overall, the results are encouraging: the most sophisticated model (based on spin−orbit hybrid DFT computations) performs best, yielding a 12.5% median relative deviation from experiment.

This paper is organized as follows. In section II details for the computational models, regarding the basis sets, and other technical details are provided. The benchmark data are provided and discussed in section III. The discussion focuses on general performance as well as on individual interesting cases or classes of compounds and classes of *J* couplings. A brief conclusion can be found in section IV.

II. Computational Details

All computations were performed with a pre-2009 release of the Amsterdam Density Functional (ADF) package.[23] Relativistic effects were incorporated in the computations with the zeroth-order regular approximation (ZORA)[24,25] using both the scalar (spin-free) and the two-component formalisms. Relativistic effects in this approach are considered in the one-electron part of the Hamiltonian (relativistic corrections to the kinetic energy of the electrons and to the electron−nucleus attraction as well as one-electron spin−orbit terms), along with relativistic corrections to the electron−electron interactions in a mean-field sense. Like in most applications of relativistic DFT NMR methodology, the spin−other-orbit term was not considered in the computations. Previous experience with two-electron spin−orbit contributions indicates that their *relative* importance decreases in comparison to their one-electron counterparts when the nuclear charges become larger,[26−28] and consequently, their effect on the coupling constants investigated here is expected to be small.

The calculations of spin−spin coupling (*J* coupling) reduced constants were performed using the CPL module of the ADF package.[8,9,12,13] "Pure", i.e., nonhybrid, DFT computations employed both the Vosko−Wilk−Nusair (VWN)[29] local density approximation (LDA) and Perdew−Burke−Ernzerhof (PBE)[30] generalized gradient approximation (GGA) terms; for simplicity, this functional will be referred to as PBE. Differences in the results compared to PBE proper, which was originally devised with a different local correlation functional, are very minor and will not affect the conclusions of this work. Hybrid DFT calculations used a corresponding PBE0 functional which includes 25% of Hartree−Fock exchange.[31] In order to facilitate the hybrid functional calculations orbital−pair density fitting techniques were applied.[12,32,33] For a better representation of the Kohn−Sham orbitals near the nuclei, the atomic nuclei were represented as Gaussian charge distributions, not as point charges as is usually done, because the effect of the nucleus representation in heavy metal spin−spin coupling calculations has been found to be significant. For details about the finite-nucleus implementation and benchmark data for *J*-coupling constants see ref 13. For the user of the software it is only required to provide a "NuclearModel Gaussian" input keyword. The nuclear radii are determined on the fly from atomic masses stored in the ADF software library.[13]

The heavy metal basis set used for obtaining the *J* couplings was an updated version of the 'JCPL' (short for *J* coupling) Slater-type orbitals (STO) basis set used in previous publications.[8,13] Since the time when some of these basis sets were first devised, the ZORA STO basis sets accompanying the ADF package have undergone minor revisions and we decided to generate a fresh set of basis sets for this benchmark study and future computational work. This JCPL basis set will accompany future releases of the program. Like previous versions, for the sixth-row elements this basis is derived from the TZ2P basis of the ADF basis set library adapted for ZORA calculations which is a valence-triple-ζ and core-double-ζ all-electron STO basis set with two sets of polarization functions. For the sixth-row elements, basis functions with exponents $\gg Z$ (Z = nuclear charge) were replaced by an even-tempered set of 9 high-exponent 1s and 2p functions along with a set of accompanying density-fit functions. A ratio of 1.69 has been used to form the even-tempered set in order to reach exponents around 10 000 with relatively few functions. Previous work showed good performance of basis sets derived in this way.[13,15] Moreover, in finite nucleus computations, these basis sets yielded reasonably well-converged results with respect to the high-exponent augmentation without causing numerical problems,[13] and thus, they represent an economical yet reasonably accurate choice for routine computations. For lighter elements, four 1s basis functions with exponents 2 Z, 3 Z, 4 Z, and 100 Z were added following a recipe given by Watson et al.[34] but with corresponding density fit functions added.[15] Atom types not involved in spin−spin couplings were represented using a double-ζ all-electron STO basis set with one set of polarization functions for all atoms (DZP of the ADF basis set library). No frozen cores were used.

For verification, all coupling constants were also computed with the older version of the JCPL basis and with the basis TZ2P3 from ref 13, which was constructed in a similar way as JCPL but with STO exponents reaching 3×10^4 for the sixth-row metals for elements as heavy as Hg and Pb. The obtained coupling constants were very similar (the difference is less than a 1% in more than 95% of the couplings calculated with the PBE functional). In calculations of coupling constants with the TZ2P3 basis and the hybrid functional, PBE0 led to convergence problems in several compounds of Hg, W, and Pt. Convergence issues with PBE0 computations and basis sets with very high STO exponents were also noted previously in ref 13, where the basis set convergence in relativistic *J*-coupling DFT calculations was investigated. The convergence problems for very high exponent basis functions are tentatively attributed to the accuracy of the numerical integration/density fitting combination used to compute the exact exchange integrals. No convergence problems were found with the JCPL and the revised JCPL basis. Due to the similarity of the results it was decided only to report data obtained with the updated JCPL basis in this work. We note, however, that both in ref 13 and during the course of the present study we noticed a slower convergence of the PBE0 *J* couplings with respect to the high-exponent augmentation, in particular with a point-nucleus model. The finite-nucleus data reported here are likely to be better converged, but the difference in basis set convergence of nonhybrid vs hybrid DFT *J* couplings of heavy atoms may warrant further investigation.

For consideration of solvent effects, the ADF implementation of the conductor-like screening model (COSMO)[35] was applied. Dielectric constants of 20.7, 37.5, 2.3, 4.8, 2.6, 8.9,

Table 1. Molecules and Spin−Spin Couplings Computed for This Work. Part 1: Hg and Pt

metal	formula	solvent[a]	one bond	two bond	others	refs
Hg	$Hg(CN)_2$	CH_3OH	Hg−C			43
	$[Hg(CN)_4]^{2-}$	gas phase[b]	Hg−C			44
	$Hg(CH_3)Cl$	CH_3Cl	Hg−C	Hg−H		45
	$Hg(CH_3)Br$	CH_3Cl	Hg−C	Hg−H		45
	$Hg(CH_3)I$	CH_3Cl	Hg−C	Hg−H		45
	$Hg(CH_3)_2$	CH_3Cl	Hg−C	Hg−H		45
	$Hg(CH_3)(CF_3)$	$\varepsilon_r = 8.0$[c]		Hg−F, Hg−H		46
	$Hg(C_6H_5)_2$	CH_2Cl_2	Hg−C	Hg−C	Hg−C[d]	43
	$Hg(CCCl)_2$	DMSO	Hg−C	Hg−C		43
	$Hg(CH_3)CCH$	C_6H_6	Hg−C[e]	Hg−C		43
	$IrCl(SnCl_3)(HgCl)(CO)(PH_3)_2$[f]	CH_3Cl		Hg−Sn, Hg−P		47
Pt	$Pt(P(CH_3)_3)_4$	THF	Pt−P			48
	$Pt(PF_3)_4$	THF	Pt−P			49
	$[Pt(CO)_3]_2^{2+}$	H_2O	Pt−Pt, Pt−C[g]	Pt−C[g]		50
	$[Pt(CN)_5]_2^{4-}$	H_2SO_4(conc)	Pt−Pt, Pt−C[g]	Pt−C[g]		51
	cis-$PtH_2(P(CH_3)_3)_2$	CH_3COCH_3	Pt−P, Pt−H			52
	trans-$PtH_2(P(CH_3)_3)_2$	CH_3COCH_3	Pt−P, Pt−H			52
	cis-$PtCl_2(P(CH_3)_3)_2$	CH_2Cl_2	Pt−P			53
	trans-$PtCl_2(P(CH_3)_3)_2$	CH_2Cl_2	Pt−P			53
	cis-$PtI_2(NH_2CH_3)_2$	CH_3COCH_3		Pt−H, Pt−C		54
	trans-$PtI_2(NH_2CH_3)_2$	CH_3COCH_3		Pt−H, Pt−C		54
	$Pt(SnCl_3)(CH_2C(CH_3)CH_2)(C_2H_4)$	CH_3Cl	Pt−Sn, Pt−C[h]	Pt−C, Pt−H[i]	Pt−H[j]	55

[a] Solvent model used in calculations. [b] Experimental value corresponds to solid-state NMR of K salt. [c] Neat liquid. A dielectric constant of 8.0 representative of organic compounds with CF_3 groups was used. [d] Both three-bond and four-bond spin−spin couplings. [e] Two different couplings for both methyl and ethinyl ligands. [f] Experimental value for $IrCl(SnCl_3)(HgCl)(CO)(P(C_6H_5)_3)_2$. [g] Both cis and trans inequivalent couplings. [h] Four inequivalent couplings. [i] Five inequivalent couplings. [j] Three-bond coupling.

5.0, 46.7, 2.3, 32.6, 2.31, 2.78, 84.0, 7.58, 2.38, and 78.39 were used to describe the solvents acetone, acetonitrile, benzene, chloroform, CS_2, dichloromethane, dimethyl ether, DMSO, Freon 113, methanol, $Pb(CH_3)_4$, $PbCl_4$, sulfuric acid, THF, toluene, and water, respectively, along with default atomic radii.

Coupling computations were performed with the following settings for the numerical integration: a global parameter of 6.0 and an atomic core parameter of 8.0. These values roughly indicate the number of significant figures for the density integration.[36] The two-component relativistic analogs of the FC, SD, PSO, and DSO terms as well as spin−orbit cross terms were included in the spin−spin couplings, except where scalar relativistic calculations were performed, in which case the (often small) SD term was neglected to lower the computational expense.

Conversions between J coupling in Hertz and reduced coupling K were based on the following gyromagnetic ratios, in 10^7 rad/(T s): 26.7522128, 6.728284, 25.18148, 10.8394, 2.624198, −10.0317, 1.1282403, 5.8385, 4.8457916, 15.5393338, 15.6921808, and 5.58046 for ^{1}H, ^{13}C, ^{19}F, ^{31}P, ^{35}Cl, ^{119}Sn, ^{183}W, ^{195}Pt, ^{199}Hg, ^{203}Tl, ^{205}Tl, and ^{207}Pb, respectively.[37] Where applicable, the couplings constant reported in this work were obtained as the average of the computed constant for every equivalent atom pair in the molecule since experimentally equivalent atoms may be nonequivalent in the calculation, for instance due to the free rotation of alkyl groups and other ligands under experimental conditions. Further, the coupling constants reported here are unsigned because the sign is not always known experimentally. We note that for the TlX series of diatomics, calculations and experiment agree in that the isotropic coupling is negative and the coupling anisotropy is positive.[12] The Supporting Information provides the full set of coupling constants, including their signs, for each of the computational models employed here.

Molecular geometries used for the spin−spin coupling computations were obtained by full DFT optimizations. The scalar ZORA operator was used to include relativistic effects along with a triple-ζ all-electron basis with polarization functions optimized for ZORA calculations (TZP from the ADF basis set library) and small frozen cores (1s frozen for C, N, O, and F, 1s−2p for Cl and P, 1s−3p for Br, 1s−4p for Sn and I, and 1s−4d for W, Pb, Pt, Tl, and Hg). The XC functional chosen for optimizations was BP, the combination of the Becke88[38] and the Perdew86[39] generalized gradient approximations (GGAs), which has been shown in benchmarks to produce reliable local minimum structures for metal complexes.[40−42] For consistency with the J-coupling computations, solvent effects were included in the optimizations by the COSMO method using the dielectric constants listed above.

III. Results and Discussion

A. Benchmark Overview and Discussion of the Scalar ZORA PBE Results. For this study a comprehensive set of experimental J-coupling data has been compiled in order to include representative cases for a wide range of heavy metal spin−spin couplings. The major NMR nuclei of the sixth row of the periodic table have been studied: W, Pt, Hg, Pb, and Tl. For the analysis a total of 47 different systems have been calculated to obtain 88 different spin−spin couplings involving one or two heavy atoms. This study includes one-bond couplings, as in previous benchmarks, but also a considerable number of two-bond couplings and some couplings through more than two bonds. A list of the selected complexes and computed couplings, with references to the experimental measurements, is provided in Tables 1 and 2. The full data set, experimental and computed coupling constants, is provided in the Supporting Information.

Table 2. Molecules and Spin−Spin Couplings Computed for This Work. Part 2: W, Pb, and Tl

metal	structure	Solvent[a]	one bond	two bond	others	refs
W	$W(CO)_6$	CH_3Cl	W−C			56
	$W(CO)_5PF_3$	$CFCl_2CF_2Cl$[b]	W−P			57, 58
	$W(CO)_5PCl_3$	$CFCl_2CF_2Cl$[c]	W−P			58
	$W(CO)_5PI_3$	$CFCl_2CF_2Cl$[c]	W−P			58
	η^5-$(C_5H_5)W(CO)_3H$	CH_3CN[d]	W−H			59
	WF_6	CS_2	W−F			60
	$W(CCH_3)(CH_2CH_3)_3$[e]	C_6H_6		W−H		61
Pb	$PbCl_4$	$PbCl_4$[f]	Pb−Cl			62
	$Pb(CH_3)_4$	$Pb(CH_3)_4$[f]	Pb−C	Pb−H		63, 64
	$Pb(CH_3)_3H$	CH_3OCH_3	Pb−H	Pb−H		64
	$Pb(CH_3)_2H_2$	CH_3OCH_3	Pb−H	Pb−H		64
	$Pb(CH_3)_2(CF_3)_2$	$\varepsilon_r = 8.0$[g]		Pb−F, Pb−H		46
	$Pb(CH_3)_3CF_3$	$\varepsilon_r = 8.0$[g]		Pb−F, Pb−H		46
	PbH_4	CH_3OCH_3[h]	Pb−H			
	$Pb_2(CH_3)_6$	C_6H_6	Pb−C	Pb−C, Pb−H	Pb−H	65
Tl	TlF	gas phase	Tl−F			66
	TlCl	gas phase	Tl−Cl			66
	TlBr	gas phase	Tl−Br			66
	TlI	gas phase	Tl−I			66
	$Tl_4(OCH_3)_4$[i]	$C_6H_5CH_3$		Tl−Tl[i]		67
	$Tl(CN)_3$	H_2O	Tl−C			68
	$Tl(CN)_2Cl$	H_2O	Tl−C			68
	$Tl(CN)Cl_2$	H_2O	Tl−C			68

[a] Solvent used in calculations. [b] Experimental solvent quoted simply as Freon. We selected Freon 113 with its intermediate ε_r. [c] Experimental solvent unknown; selected $CFCl_2CF_2Cl$ for analogy with $W(CO)_5PF_3$. [d] Experimental measurement in liquid crystal (ZLI-1132 Merck/EBBA). [e] As a model for $W(CC(CH_3)_3)(CH_2C(CH_3)_3)_3$. [f] Neat liquid. [g] Neat liquid. A dielectric constant of 8.0, representative of organic compounds with CF_3 groups, was used. [h] Experimental value not known. The value used has been extrapolated from $Pb(CH_3)_3H$ and $Pb(CH_3)_2H_2$. [i] Experimental value for $Tl_4(OC(CH_3)_3)_4$, $^{205}T-^{203}Tl$.

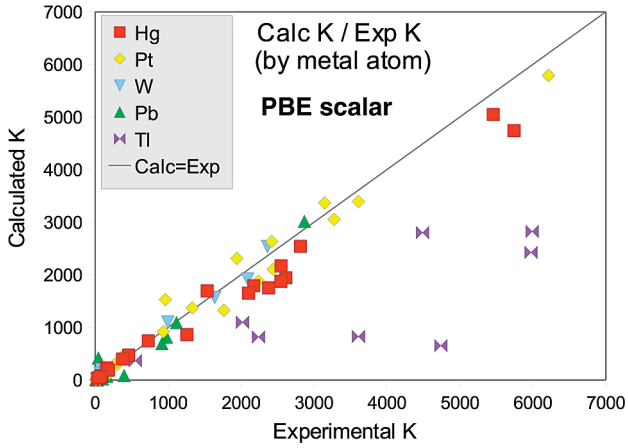

Figure 1. Computed absolute values of the reduced nuclear spin−spin coupling constants *K* versus absolute experimental values (in units of 10^{19} T^2 J^{-1}) for PBE, scalar ZORA calculations. Two coupling constants involving Sn and a heavy metal nucleus have been omitted due to their magnitude.

In Figure 1 most of the computed reduced spin−spin coupling (*J*-coupling) constants obtained from scalar ZORA computations using the nonhybrid PBE functional are plotted vs experiment. A good correlation can be observed for most of the computed couplings, although there are several large disagreements, in particular for the Tl systems. Apart from these outliers, the correlation appears to be reasonable at the scale of the plot.

Since the data set spans several orders of magnitude and includes some severe outliers one needs to be careful with assessing the performance numerically based on average or rms deviations. An overall assessment of the agreement with experiment can be obtained by comparing the average and median of the unsigned deviation for both the absolute and the relative errors, with associate variability measures as the standard deviation (SD) around the average and median unsigned deviation (MD)[79] around the median (see Table 3).

The most significant discrepancy between theory and experiment is the systematic underestimation of the coupling constant in the thallium systems. This is expected because previous works[12,15] have shown that in these Tl compounds the inclusion of spin−orbit coupling is crucial. The relative errors for couplings involving Pb are of similar magnitude. In this case there are a number of small coupling constants that are not well described at the scalar ZORA PBE level of theory. Besides Tl and Pb the most significant absolute deviation of the coupling constant is observed in the complex $IrCl(SnCl_3)(HgCl)(CO)(PH_3)_2$. For its huge Hg−Sn two-bond coupling constant, which is outside the plot range of Figure 1, the deviation of 11 710 × 10^{19} T^2 J^{-1} with respect to the experiment represents 23% of the total coupling of −50 838 × 10^{19} T^2 J^{-1}.[47] This and most of the other significant discrepancies and selected cases will be discussed later in section III.E. Couplings involving Hg and a light ligand in linear Hg(II) complexes are reasonably close to experiment. We note already here that the hybrid DFT results for Hg−C couplings reported below agree very well with experiment. It should be noted, however, that explicit solvation was demonstrated to increase Hg−C couplings in linear Hg(II) complexes quite significantly,[21] and therefore, it is likely that an error compensation regarding the complexes structure, solvation effects on structure and *J* coupling, and approximations in the density functional, is influential both in the present computations as well as in previous work. By extrapolating the trends regarding solvation effects that were reported in ref 21 a dynamic model with explicit solvation

Table 3. Statistical Error Parameters for the PBE, ZORA Scalar Calculations

	absolute deviation[a]				relative deviation[a]			
	ΔK_{mean}	SD[b]	ΔK_{median}	MD[c]	ΔK^{rel}_{mean}	SD[b]	ΔK^{rel}_{median}	MD[c]
total	513.3	1462.7	71.1	68.4	39.6%	90.2%	17.6%	11.5%
Hg	753.4	2352.5	158.5	153.4	16.9%	10.3%	17.0%	7.3%
Pt	233.7	685.7	32.5	30.4	23.3%	23.5%	13.6%	7.5%
W	73.8	57.0	70.3	42.8	35.7%	46.2%	10.3%	8.7%
Pb	98.1	111.7	25.7	19.1	100.2%	192.9%	68.5%	18.3%
Tl	2226.0	2536.9	2235.2	1122.8	57.0%	55.2%	56.2%	14.5%
one bond	676.7	1043.6	324.7	241.1	46.7%	122.9%	18.3%	9.5%
two bond	352.0	1920.2	14.7	9.3	32.9%	33.3%	18.2%	9.4%
longer	4.3	2.8	3.7	1.9	18.7%	14.8%	11.4%	6.3%

[a] Mean and median unsigned absolute and relative deviations from experiment. Absolute deviations in 10^{19} T^2 J^{-1}. Relative deviation calculated as $\Delta K^{rel} = |(K_{calcd} - K_{exp})/K_{exp} \times 100\%|$ with unsigned K values. [b] Standard deviation (SD) calculated as $((1/N)\Sigma_{i=1}^{N}(\Delta K_i - \Delta K_{mean}))^{1/2}$. [c] Median unsigned deviation (MD) obtained as median$_i$ ($|\Delta K_i - \Delta K_{med}|$).

might eventually lead to an overestimation of these J couplings with respect to experiment at the level of theory employed for this study. However, this will have to be demonstrated explicitly in future work. Unlike previous computations,[21] here the full GGA response kernel is considered in the computations, along with the continuum model, the revised JCPL basis, and finite nucleus corrections, and the geometries were optimized which is an important factor. The combination of these effects lead to a less strong underestimation of Hg−C couplings calculated with a GGA functional when explicit solvation is omitted, as compared to previous work, which is beneficial for the performance of the computational model used here.

Overall, the pronounced discrepancy between average and median errors in the summary for all metals in Table 1 indicates that at this level of theory a considerable number of outliers taint the otherwise reasonable appearance of the data set in Figure 1. Regarding the performance of the computations for two-bond and higher couplings, the results are promising since the relative median deviations from experiment are comparable to the one-bond couplings.

B. Functional: PBE vs PBE0. Using a hybrid functional (PBE0) results in a clear improvement of the overall agreement of the computed coupling constants with experiment as can be observed in both the plot of computed couplings vs experiment (Figure 2) and the statistical parameters (Table 4). The outliers for Tl remain at this scalar relativistic level of theory. Most of the coupling constants are better represented with this functional (57 of the total 88 coupling constants improve toward experiment). However, when computing the overall deviation by metal, for molecules containing Hg, Pb, and W, worse average results are observed in the hybrid-DFT calculations. For mercury, however, this trend is coming from an individual exception, the huge ^2J(Hg−Sn) coupling constant in $IrCl(SnCl_3)(HgCl)(CO)(PH_3)_2$. It has a great absolute error in both sets of scalar relativistic calculations. Its calculated value is further away from experiment with PBE0, with an unsigned deviation around 100 times the second largest error among the Hg couplings. If this coupling is discarded, a very significant improvement of the overall mean deviations is obtained for both the PBE0 and the PBE sets of calculations. The change from the PBE calculations (average deviation = 255.4 10^{19} T^2 J^{-1}) to PBE0 (average deviation = 82.1) shows the general trend of improvement for Hg when including exact exchange

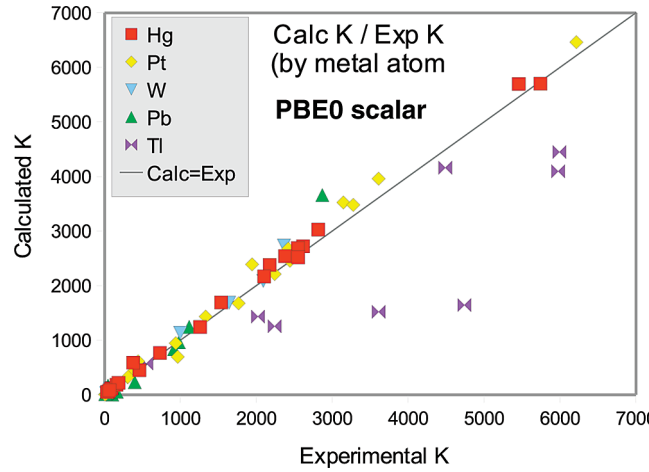

Figure 2. Computed vs experimental reduced couplings (in 10^{19} T^2 J^{-1}) for PBE0, scalar ZORA calculations. See also caption of Figure 1.

in the functional with results closer to experiment in 14 of the 23 calculated K (Hg−X) couplings. Regarding the W and Pb computations, a general trend is not observed in the absolute mean deviation. For example, the number of improved results for the W complexes (4) and of worse results (3) are similar, and so the overall accuracy for scalar relativistic PBE vs PBE0 is comparable. However, an improvement in the relative deviations is observed in the Pb and W results due to improvements of the calculations of the small J-coupling constants for which the relative error with PBE is often quite large. The small couplings will be discussed in more detail further below.

Regarding the relation of the coupling path length to the performance of the model, the hybrid functional yields better agreement with experiment for the one-bond couplings than for two- and multibond couplings. Although the inclusion of exact exchange in the functional reduces the one-bond coupling overall deviations to less than one-half, the agreement with experiment becomes worse for the long-range couplings (three and four bond). The improvement of the performance mainly for the one-bond couplings is also clearly visible in the relative mean and median errors. In the case of two-bond couplings, the mean absolute deviation increases from PBE to PBE0, but it is mostly due to the individual bad result of the Hg−Sn coupling, as mentioned above. When omitting the Hg−Sn coupling from the test

Table 4. Statistical Error Parameters for the PBE0, ZORA Scalar Calculations

	absolute deviation[a]				relative deviation[a]			
	ΔK_{mean}	SD[b]	ΔK_{median}	MD[c]	ΔK^{rel}_{mean}	SD[b]	ΔK^{rel}_{median}	MD[c]
total	476.5	2500.5	33.9	30.9	22.4%	33.2%	12.2%	9.3%
Hg	1093.8	4746.0	32.9	17.0	16.4%	13.5%	7.5%	6.0%
Pt	118.9	238.7	13.6	10.8	15.1%	15.1%	10.8%	6.4%
W	87.8	122.9	35.0	27.3	19.1%	16.3%	15.7%	12.8%
Pb	98.8	186.7	28.2	27.1	42.4%	65.2%	20.2%	11.3%
Tl	1317.4	1598.9	1265.1	750.9	33.1%	35.9%	30.3%	18.3%
one bond	363.3	711.2	132.1	120.8	19.5%	41.0%	8.0%	18.2%
two bond	678.8	3890.0	8.5	8.4	25.7%	21.8%	18.2%	14.1%
longer	14.1	12.1	11.3	7.5	19.0%	11.5%	24.0%	10.4%

[a] Mean and median unsigned absolute and relative deviations. Absolute deviations in 10^{19} T^2 J^{-1}. See footnotes of Table 3 for details. [b] Standard deviation (SD). [c] Median unsigned deviation (MD).

Table 5. Statistical Error Parameters for the PBE, ZORA Spin−Orbit Calculations

	absolute deviation[a]				relative deviation[a]			
	ΔK_{mean}	SD[b]	ΔK_{median}	MD[c]	ΔK^{rel}_{mean}	SD[b]	ΔK^{rel}_{median}	MD[c]
total	466.1	1142.0	69.2	65.5	40.7%	97.1%	20.6%	11.6%
Hg	665.6	1633.6	171.0	170.4	20.0%	11.5%	17.8%	6.3%
Pt	290.2	861.0	35.4	32.2	24.5%	21.7%	16.2%	10.5%
W	99.3	80.9	50.0	45.8	38.4%	50.4%	12.1%	8.2%
Pb	122.4	130.1	53.9	39.0	106.7%	209.7%	56.7%	32.8%
Tl	1649.0	2068.0	1587.5	1092.7	38.5%	39.7%	38.7%	10.4%
one bond	662.6	1181.5	362.2	359.0	47.6%	132.1%	22.2%	11.8%
two bond	255.5	1359.7	17.2	14.0	34.1%	33.8%	19.9%	10.1%
longer	4.0	3.4	3.2	2.4	17.1%	16.5%	14.2%	8.3%

[a] Mean and median unsigned absolute and relative deviations. Absolute deviations in 10^{19} T^2 J^{-1}. See footnotes of Table 3 for details. [b] Standard deviation (SD). [c] Median unsigned deviation (MD).

Table 6. Statistical Error Parameters for the PBE0, ZORA Spin−Orbit Calculations

	absolute deviation[a]				relative deviation[a]			
	ΔK_{mean}	SD[b]	ΔK_{median}	MD[c]	ΔK^{rel}_{mean}	SD[b]	ΔK^{rel}_{median}	MD[c]
total	352.2	1934.4	43.4	39.0	22.4%	36.1%	12.5%	9.4%
Hg	856.8	3686.8	35.0	32.7	14.8%	12.5%	10.1%	7.4%
Pt	111.9	246.7	19.0	17.5	16.6%	15.0%	11.5%	7.9%
W	70.6	74.9	44.1	37.5	15.0%	16.0%	8.2%	5.5%
Pb	68.2	72.0	30.0	26.3	49.0%	72.2%	26.5%	16.5%
Tl	737.1	1019.6	487.0	258.8	22.0%	29.9%	13.3%	8.9%
one bond	235.8	465.3	96.7	87.6	17.2%	45.2%	7.4%	17.5%
two bond	545.2	3023.7	10.2	6.5	29.3%	21.3%	25.1%	11.8%
longer	11.3	9.2	9.1	5.2	18.3%	9.7%	22.3%	9.9%

[a] Mean and median unsigned absolute and relative deviations. Absolute deviations in 10^{19} T^2 J^{-1}. See footnotes of Table 3 for details. [b] Standard deviation (SD). [c] Median unsigned deviation (MD).

set the mean absolute deviations are comparable within the uncertainties of the averages (absolute average = 27.4 for PBE and 31.1 for PBE0), showing a similar performance in this case for both functionals for the two-bond couplings.

C. Spin−Orbit Effects. The inclusion of spin−orbit (SO) coupling in the ZORA computations has no systematic effect on the accuracy of the couplings when considering the whole data set. The calculation results are summarized in Tables 5 and 6 and Figures 3 and 4. In the PBE0 calculations, for example, 44 of the 88 computed couplings are improved by including SO coupling in the formalism. As a result, the absolute average deviation is improved but not the median, and the relative errors are very similar. As pointed out earlier, a systematic and large improvement is obtained for some of the couplings involving the Tl atom. SO effects on other molecules are less significant and variable, even decreasing the agreement with experiment in some examples. For most metals, the overall effect of including SO coupling is different in hybrid and pure DFT calculations: in 34 of the computed couplings spin−orbit coupling improves the result only for one of the functionals.

The SO effect will be analyzed separately for the different kinds of couplings under consideration here. As a general finding, the overall deviations listed in Table 6 document that the combination of the PBE0 functional with the spin−orbit ZORA relativistic formalism yields the best agreement with experiment among the computational models tested here and that it is an overall well-performing method for this set of coupling constants. The results are somewhat reassuring because this computational model is also the most sophisticated among those tested here. Incidentally, it is the most expensive model too in terms of the required computing resources.

For the Hg compounds, including SO effects always reduces the absolute mean deviation from experiment, but the median of the absolute unsigned error increases. In the

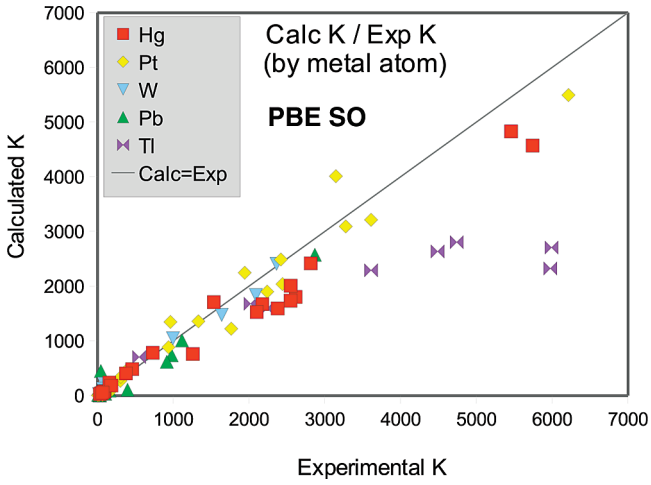

Figure 3. Computed vs experimental reduced couplings (in 10^{19} T^2 J^{-1}) for PBE, spin−orbit ZORA calculations. See also caption of Figure 1.

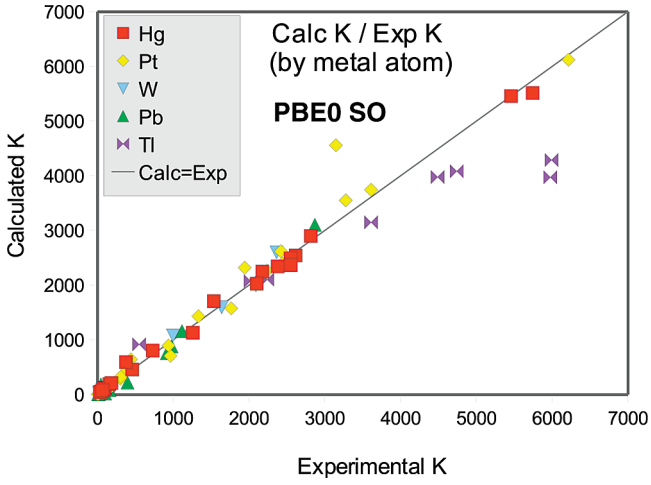

Figure 4. Computed vs experimental reduced couplings (in 10^{19} T^2 J^{-1}) for PBE0, spin−orbit ZORA calculations. See also caption of Figure 1.

PBE calculation most of the individual Hg couplings (19 out of 23) have slightly less good agreement with experiment when including SO coupling, but the improvement in the very large ^2J(Hg−Sn) dominates the overall statistics. In the PBE0 calculations it is also the ^2J(Hg−Sn) coupling that dominates the absolute deviations, but here also the general trend is that SO coupling improves the results slightly. At the PBE0 level, 15 of the Hg coupling constants improve with respect to experiment when SO effects are considered. However, the average improvement (excluding the ^2J(Hg−Sn) coupling) is just on the order of 10×10^{19} T^2 J^{-1}.

For the Pt complexes the inclusion of SO coupling worsens the agreement with experiment for most of the J couplings (for 21 couplings with PBE and 20 with PBE0 out of a total of 34). On the other hand, the absolute mean deviation from experiment is smaller for the PBE0 calculations when comparing scalar with SO results but only by about 7×10^{19} T^2 J^{-1}. We emphasize the case of the Pt−Pt coupling in the $[Pt(CN)_5]_2^{4-}$ complex: In this case inclusion of SO coupling yields a large difference between theory and experiment (in PBE0 calculation by more than 1000×10^{19} T^2 J^{-1}, which is 33% of the experimental value). This result highlights the difficulty of assessing approximate computational results in which potentially important effects are not included: a good agreement of scalar relativistic data with experiment might lead to the conclusion that the magnitude of SO effects is small, which is not correct in this case.

For complexes with W, opposite behaviors with respect to SO effects are observed with the two functionals. Spin−orbit effects in combination with the hybrid functional clearly improve the results, but they render the agreement of PBE with experiment worse. The combination of PBE0 with the SO relativistic formalism yields overall very good results, with a median relative deviation of 10%. These are the best results for any of the metals in terms of both absolute and relative deviations.

For compounds of Pb, it also depends on the functional whether SO effects improve the agreement with experiment or not. In the nonhybrid PBE calculations both relative and absolute deviations increase upon inclusion of SO effects. Despite the fact that the PBE0 absolute mean deviation is lower with SO coupling, there is an increase in the relative errors compared to scalar relativistic calculations, showing that spin−orbit coupling mainly improves the larger J couplings but renders the results worse for some of the Pb couplings with small magnitudes.

For complexes with Tl, the increase of the accuracy of the calculations upon the inclusion of SO coupling is very significant for the TlX (X = halide) series for both functionals. However, the SO effect in the $Tl(CN)_nCl_{(3-n)}$ series and for $Tl_4(OCH_3)_4$ is to increase the deviation from experiment. Since the gain in accuracy for some of the systems is quite significant (around 40% of the experimental value) while the loss of accuracy for the cyanide series is relatively minor (around 3%), the overall result is a clear improvement of the Tl couplings upon inclusion of SO coupling in the computations. Therefore, for the Tl systems the best results for the reduced NMR spin−spin coupling constants are obtained from the spin−orbit relativistic hybrid PBE0 functional calculations.

Focusing on the one-bond couplings, despite the fact that the absolute mean deviation is always smaller when spin−orbit coupling is included, in the PBE calculations the absolute median and both the relative mean and the median deviations increase slightly. The meaning of this is that some of the worst results are improving, but there is somewhat less good agreement with experiment for some of the coupling constants that agreed quite well with experiment in the scalar relativistic calculations. Overall, with PBE there is only an improvement toward experiment for one-third of the couplings upon including SO coupling. When spin−orbit coupling is applied in combination with the hybrid functional, most of the results improve toward experiment, and as a consequence, all the statistic parameters improve.

For the two-bond couplings, although the absolute averages show better agreement with experiment when SO coupling is included, this is mainly due to the Hg−Sn case. If it is excluded from the test set the mean absolute deviations are slightly higher but just by 2×10^{19} T^2 J^{-1} for PBE and 11

Table 7. Statistical Error Parameters for Gas-Phase PBE0 ZORA Spin−Orbit *J*-Coupling Calculations[d]

	absolute deviation[b]				relative deviation[b]			
	ΔK_{mean}	SD[c]	ΔK_{median}	MD[d]	ΔK^{rel}_{mean}	SD[c]	ΔK^{rel}_{median}	MD[d]
total	241.9	549.2	44.5	43.2	24.4%	36.5%	13.9%	10.4%
Hg	188.7	266.9	61.0	55.1	13.5%	12.8%	13.8%	4.7%
Pt	186.0	417.1	31.9	31.5	23.2%	24.3%	11.6%	10.4%
W	65.9	64.7	33.9	26.6	18.3%	16.1%	8.7%	7.3%
Pb	53.7	68.8	18.0	9.9	42.8%	70.5%	25.2%	15.7%
Tl	1163.0	1695.1	559.1	463.0	29.5%	37.9%	23.6%	19.2%
one bond	396.6	795.7	137.4	129.7	22.6%	44.7%	10.9%	12.0%
two bond	61.3	155.4	10.8	6.1	27.4%	25.4%	21.5%	10.4%
longer	10.3	9.3	7.6	5.0	14.1%	6.4%	16.4%	4.8%

[a] Same as Table 6 and Figure 4 but without application of the continuum solvent model in the *J*-coupling computations (optimized geometries were the same as in Table 4 and Figure 4). [b] Mean and median unsigned absolute and relative deviations. Absolute deviations in 10^{19} T^2 J^{-1}. See footnotes of Table 3 for details. [c] Standard deviation (SD). [d] Median unsigned deviation (MD).

$\times$ 10^{19} T^2 J^{-1} for PBE0. At the same time the absolute median and both relative deviations worsen slightly.

The effect of SO coupling in the statistical parameters for longer range couplings is quite small, and general trends are not observed (the data set is also small, and not too much significance should be attributed to minor differences in the statistical parameters for different sets of computations). For the few data points we have available, one-half of the coupling constants improve and the other half become worse in comparison with experiment when SO coupling is included.

D. Overall Importance of the Solvent Model. One might wonder how large the influence from the continuum solvent model is in the calculations. In Table 7 the statistical data are provided for calculations at the PBE0 ZORA spin−orbit level but without the continuum model. The optimized geometries are the same as those used in all other computations in this paper. If we focus on the relative deviations from experiment, it is seen that the performance of the gas-phase calculations is not significantly worse than the calculations with the COSMO solvent model when taking the standard deviations of the mean and median into consideration. The breakdown per metal reveals similar performance of the gas-phase computations for Hg, Pt, and W, as quantified by the median relative deviations. The trends in the absolute deviations are strongly influenced by the Hg−Sn coupling (see the apparently remarkable improvement of the overall absolute average errors). As will be discussed in the next section, the large-magnitude Hg−Sn coupling tends to dominate the mean deviations in our data set and in the case of the gas-phase calculations this coupling constant happens to be close to experiment. Given the sensitivity of this coupling constant to the computational model, this Hg−Sn-bonded compound deserves further investigation. For the trigonal Tl systems such as $Tl(CN)_2Cl$ we will demonstrate in the next section that a dynamic study with explicit solvent molecules (water) is likely to be necessary in order to reproduce the experimental *J* couplings within a 10% margin of error. Previous work by our group has reported large explicit solvent effects on *J* couplings in metal complexes with Tl.[14,18] The breakdown per metal in Table 5, in comparison with the COSMO data in Table 4, already shows improvements for Tl from the continuum model. However, just like in other Tl complexes that we investigated in the past, the continuum model alone, without explicit solvent, is not sufficient to reproduce experimental data obtained in solution.

E. Some Individual Cases. *1. Tl.* The *J* couplings in the Tl compounds are quite strongly dependent on the computational model. The pronounced SO effects have already been highlighted. The findings in this work further echo conclusions from previous studies of Pt−Tl coupling constants carried out in our group[14] in which a strong sensitivity of the results with respect to the computational model was noted. A spin−orbit relativistic formalism as well as the use of a hybrid functional appears to be overall beneficial for the computation of NMR parameters in Tl complexes. However, we pointed out already that spin−orbit coupling does not improve the results for some cyanide thallium complexes.

The *J* coupling in the Tl−X series of diatomics is particularly strongly affected by SO coupling. Figure 4 (see also the Supporting Information) shows that despite the strong improvement toward experiment the SO PBE0 results are still somewhat too small in magnitude. This is in part due to the structural aspect of the computational model: the BP-optimized bond lengths are larger than the experimentally determined equilibrium distances reported in ref 69. Figure 5 demonstrates that when experimental equilibrium distances are used for the TlX series the computed coupling magnitudes slightly overshoot the experimental ones. Remaining deviations from experiment are tentatively attributed to the approximations in the density functional as one of the major remaining sources of error.

For some examples, such as $Tl(CN)_2Cl$, the deviation between computations and experiment remain quite large even for the PBE0 SO calculation. It is likely that solvent effects need to be modeled explicitly in order to obtain *J* couplings that are within 5−10% of the experimental data. Previously, the importance of including solvent effects with explicit solvent molecules was demonstrated for complexes with vacant sites in their first coordination sphere.[14,18,21] In order to investigate this issue, for the $Tl(CN)_2Cl$ complex an additional set of calculations was performed but now considering explicitly the solvent. Two water molecules, one above and one below the metal−ligand plane, were added in the calculations. The results show some improvement, reducing the deviation from experiment from 26% to 18%

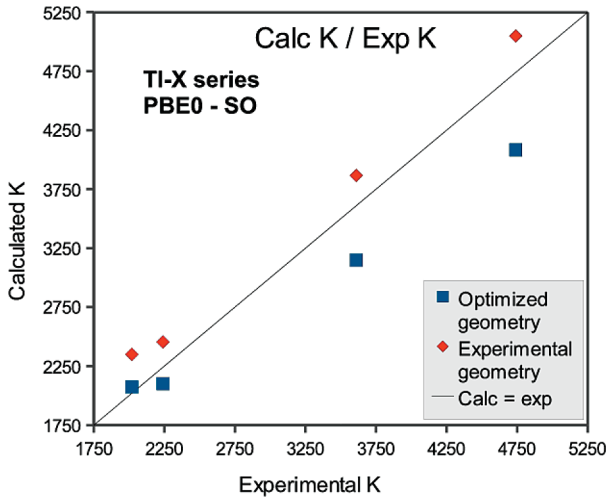

Figure 5. Computed vs experimental reduced couplings (in 10^{19} T^2 J^{-1}) of the Tl−X (X = F, Cl, Br, I) diatomics for PBE0, spin−orbit ZORA calculations: Optimized (BP/ZORA/TZP, blue square markers) and experimental bond lengths (orange diamond markers).

in the spin-free PBE0 calculation (which yields the best results for this molecule).

2. Small Couplings. It has been pointed out above that the hybrid functional performance is superior for most of the smallest coupling constants. This is shown explicitly in Figure 6 where the coupling constants are plotted on a smaller scale. In particular, for a group of very small Pb couplings, with magnitudes of less than 50 × 10^{19} T^2 J^{-1}, the inclusion of HF exchange in the functional brings the results closer to experiment. The same behavior is observed for the SO relativistic computations. For the small coupling constants, which may afford large relative deviations from experiment, the hybrid functional appears to be particularly beneficial.

3. Huge Sn Couplings. In this study, the performance of the functionals was also tested for some very large *J*-coupling constants. In general, reduced couplings involving Hg tend to be very large, and the 'world record' holders among coupling constants are therefore not surprisingly Hg−Hg one-bond couplings.[19,70−72] Herein, we considered some very large coupling constants between a heavy metal and the Sn nucleus. As seen above, for the largest coupling, ^2J(Hg−Sn) in $IrCl(SnCl_3)(HgCl)(CO)(PH_3)_2$, the deviation from experiment is always large, both in absolute and relative terms. However, this is not a general behavior for Sn couplings. For example, the ^1J(Pt−Sn) coupling is within 1% of the experimental value (absolute deviation = 240 × 10^{19} T^2 J^{-1}). Also, the behavior of these couplings with respect to the functional is different: For the Hg−Sn coupling, the error is larger with PBE0 while the Pt−Sn coupling constant is closer to experiment with the hybrid functional.

4. Model Compounds. In order to reduce the computational resource requirements for some of the calculations a few large compounds considered in this study have been replaced by smaller models. These complexes are $IrCl(SnCl_3)(HgCl)(CO)(P(C_6H_5)_3)_2$, $W(CC(CH_3)_3)(CH_2C(CH_3)_3)_3$, and $Tl_4(OC(CH_3)_3)_4$). For the Hg system, a model compound was calculated where triphenylphosphine was replaced by PH_3. For the other systems methyl has replaced *tert*-butyl. The models for the ligands along with a missing treatment of solvent and dynamic effects are likely responsible for part of the deviations between the computations and experiment. Whether the approximations for the ligands have a large impact, however, is unclear at this time. The Hg system has been discussed in the previous paragraph. For the W and Tl compounds, the absolute mean deviation from experiment is 61.3 × 10^{19} T^2 J^{-1}, and the relative mean deviation is 8.4% for the PBE spin−orbit calculations which agree best with experiment. The corresponding data are 197.4 × 10^{19} T^2 J^{-1} and 53.7%, respectively, for the PBE0 spin−orbit computations which agree worst with experiment. The performance of the calculations for these systems is similar to the average performances for the whole test set for three of the four computational models, except for PBE0 spin−orbit where $^2J(^{203}Tl-^{205}Tl)$ is strongly overestimated with this method.

IV. Concluding Remarks and Outlook

It is not easy to achieve good agreement between computations and experiment for heavy atom *J*-coupling constants in heavy metal systems. It has previously been pointed out that relativistic effects serve as a kind of 'magnifying glass' for subtle effects in the bonding in such systems,[4] which is one of the reasons for these difficulties. Any approximation in the computational model is 'felt' by this sensitive molecular property. Nonetheless, from the results in this benchmark study, a reasonably good performance of the hybrid functional PBE0 in the computations of spin−spin coupling constant with heavy metal atoms can be observed.

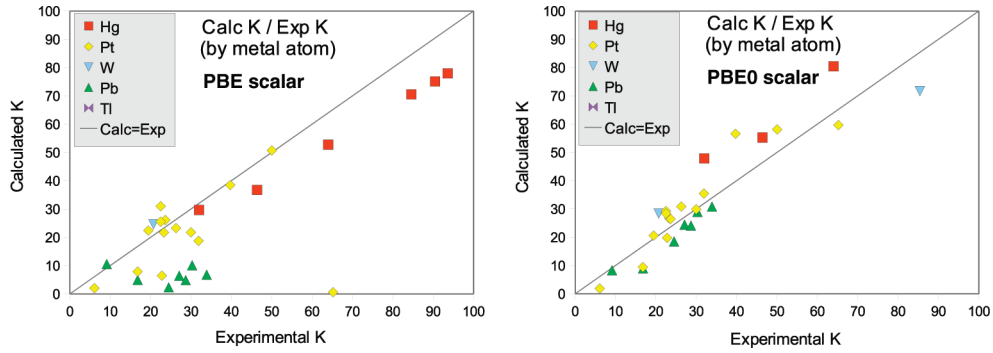

Figure 6. Computed vs experimental reduced couplings (in 10^{19} T^2 J^{-1}) for scalar ZORA, PBE vs PBE0, for |*K*| < 100: (left) PBE, (right) PBE0.

The good performance includes the representation of two-bond coupling constants in heavy metal systems, which have not previously been benchmarked. The inclusion of spin−orbit coupling in the calculations does not consistently lead to improved agreement with experiment across the whole test set, and its application must be analyzed more carefully. This finding can only mean that exclusion of SO coupling is in some cases balancing errors resulting from other approximations.

The systematic use of DFT-optimized structures is considered beneficial for the purpose of this paper since it makes all computations subject to similar potential deficiencies in the geometries. This way, the errors in the *J* couplings due to the optimizations are part of the whole assessment of each computational model. Overall, the most sophisticated computational model in which the *J* couplings are computed with SO coupling and with the hybrid functional performs best on average with a 12.5 ± 9.4% median deviation. Outliers are still present in this computational model, as evidenced by the larger relative mean absolute error of 22.4%, which also has a large standard deviation. This computational model should be considered satisfactory for discussing trends in the *J* couplings for a wide range of sixth-row heavy atom spin−spin coupling constants and to analyze the results in chemically meaningful terms. Much better quantitative agreement with experiment, i.e., setting a goal of reducing these deviations by an order of magnitude, is likely to require dynamic models including sophisticated treatment of solvent effects along with better density functionals (or explicitly correlated wave function methods), more flexible basis sets, and possibly a more accurate treatment of relativistic effects beyond ZORA. Regarding the latter, numerical and basis set DFT calculations of ZORA hyperfine integrals of heavy atom semicore and valence orbitals needed for the calculations of *J* coupling have revealed that they are within less than 1% deviation of the four-component relativistic results.[73] Since *J* coupling is a valence property (i.e., in heavy element compounds the contributions from atomic core orbitals for which ZORA affords significant errors are negligible[15,74]), approximations other than the relativistic model are likely to be of higher importance.

Acknowledgment. We acknowledge support from the Center of Computational Research at SUNY Buffalo and financial support of this research from the National Science Foundation (grant no. CHE-0447321). The Spanish agency MICINN is acknowledged for a fellowship to S. Moncho and for providing the financial support for his participation in this project.

Supporting Information Available: Optimized geometries for all systems in the test set, and calculated and experimental *J* couplings. This material is available free of charge via the Internet at http://pubs.acs.org.

References

(1) Facelli, J. C. Shielding Calculations. In *Encyclopedia of Nuclear Magnetic Resonance*; Grant, D. M., Harris, R. K., Eds.; John Wiley & Sons: Chichester, 2002; Vol. 9, pp 332−333.

(2) Helgaker, T.; Jaszuński, M.; Ruud, K. *Chem. Rev.* **1999**, *99*, 293–352.

(3) Kowalewski, J. *Annu. Rep. NMR Spectrosc.* **1982**, *12*, 81–176.

(4) Autschbach, J. *Coord. Chem. Rev.* **2007**, *251*, 1796–1821.

(5) Autschbach, J.; Ziegler, T. *Coord. Chem. Rev.* **2003**, *238/239*, 83–126.

(6) Autschbach, J.; Zheng, S. *Annu. Rep. NMR Spectrosc.* **2009**, *67*, 1–95.

(7) Enevoldsen, T.; Visscher, L.; Saue, T.; Jensen, H. J. A.; Oddershede, J. *J. Chem. Phys.* **2000**, *112*, 3493–3498.

(8) Autschbach, J.; Ziegler, T. *J. Chem. Phys.* **2000**, *113*, 936–947.

(9) Autschbach, J.; Ziegler, T. *J. Chem. Phys.* **2000**, *113*, 9410–9418.

(10) Filatov, M.; Cremer, D. *J. Chem. Phys.* **2004**, *120*, 11407–11422.

(11) Melo, J. I.; Ruiz de Azúa, M. C.; Peralta, J. E.; Scuseria, G. E. *J. Chem. Phys.* **2005**, *123*, 204112–7.

(12) Autschbach, J. *J. Chem. Phys.* **2008**, *129*, 094105–9. Autschbach, J. Erratum. *J. Chem. Phys.* **2009**, *130*, 209901.

(13) Autschbach, J. *ChemPhysChem* **2009**, *10*, 2274–2283.

(14) Le Guennic, B.; Matsumoto, K.; Autschbach, J. *Magn. Reson. Chem.* **2004**, *42*, S99–S116.

(15) Autschbach, J. *J. Chem. Phys.* **2007**, *127*, 124106–11.

(16) Boshaalaa, A. M. A.; Simpson, S. J.; Autschbach, J.; Zheng, S. *Inorg. Chem.* **2008**, *47*, 9279–9292.

(17) Autschbach, J.; Le Guennic, B. *J. Chem. Educ.* **2007**, *84*, 156–171.

(18) Autschbach, J.; Le Guennic, B. *J. Am. Chem. Soc.* **2003**, *125*, 13585–13593.

(19) Autschbach, J.; Sterzel, M. *J. Am. Chem. Soc.* **2007**, *129*, 11093–11099.

(20) Chen, W.; Liu, F.; Matsumoto, K.; Autschbach, J.; Le Guennic, B.; Ziegler, T.; Maliarik, M.; Glaser, J. *Inorg. Chem.* **2006**, *45*, 4526–4536.

(21) Autschbach, J.; Ziegler, T. *J. Am. Chem. Soc.* **2001**, *123*, 3341–3349.

(22) Autschbach, J.; Ziegler, T. *J. Am. Chem. Soc.* **2001**, *123*, 5320–5324.

(23) Baerends, E. J. *Amsterdam Density Functional, SCM*; Theoretical Chemistry, Vrije Universiteit: Amsterdam, The Netherlands, http://www.scm.com.

(24) van Lenthe, E.; Baerends, E. J.; Snijders, J. G. *J. Chem. Phys.* **1994**, *101*, 9783–9792.

(25) van Lenthe, E.; Ehlers, A.; Baerends, E. J. *J. Chem. Phys.* **1999**, *110*, 8943–8953.

(26) Okada, S.; Shinada, M.; Matsuoka, O. *J. Chem. Phys.* **1990**, *93*, 5013–5019.

(27) Ishikawa, Y.; Nakajima, T.; Hada, M.; Nakatsuji, H. *Chem. Phys. Lett.* **1998**, *283*, 119–124.

(28) Vaara, J.; Ruud, K.; Vahtras, O.; Ågren, H.; Jokisaari, J. *J. Chem. Phys.* **1998**, *109*, 1212–1222.

(29) Vosko, S. H.; Wilk, L.; Nusair, M. *Can. J. Phys.* **1980**, *58*, 1200–1211.

(30) Perdew, J. P.; Burke, K.; Ernzerhof, M. *Phys. Rev. Lett.* **1996**, *77*, 3865–3868.

(31) Adamo, C.; Barone, V. *J. Chem. Phys.* **1999**, *110*, 6158–6170.

(32) Ye, A.; Patchkovskii, S.; Autschbach, J. *J. Chem. Phys.* **2007**, *127*, 074104−13.

(33) Bryce, D.; Autschbach, J. *Can. J. Chem.* **2009**, *87*, 927–941.

(34) Watson, M. A.; Handy, N. C.; Cohen, A. J.; Helgaker, T. *J. Chem. Phys.* **2004**, *120*, 7252–7261.

(35) Pye, C. C.; Ziegler, T. *Theor. Chem. Acc.* **1999**, *101*, 396–408.

(36) te Velde, G.; Baerends, E. J. *J. Comput. Phys.* **1992**, *99*, 84–98.

(37) WebElements, http://www.webelements.com.

(38) Becke, A. D. *Phys. Rev. A* **1988**, *38*, 3098–3100.

(39) Perdew, J. P. *Phys. Rev. B* **1986**, *33*, 8822–8824.

(40) Waller, M. P.; Braun, H.; Hojdis, N.; Bühl, M. *J. Chem. Theory Comput.* **2007**, *3*, 2234–2242.

(41) Bühl, M.; Reimann, C.; Pantazis, D. A.; Bredow, T.; Neese, F. J. *Chem. Theory Comput.* **2008**, *4*, 1449–1459.

(42) Furche, F.; Perdew, J. P. *J. Chem. Phys.* **2006**, *124*, 044103−27.

(43) Sebald, A.; Wrackmeyer, B. *J. Magn. Reson.* **1985**, *63*, 397–400.

(44) Wu, G.; Kroeker, S.; Wasylishen, R. E. *Inorg. Chem.* **1995**, *34*, 1595–1598.

(45) Brown, A. J.; Howarth, O. W.; Moore, P. *J. Chem. Soc., Dalton Trans.* **1976**, 1589–1592.

(46) Eujen, R.; Lagow, R. J. *J. Chem. Soc., Dalton Trans.* **1978**, 541–544.

(47) Kretschmer, M.; Pregosin, P. S. *J. Org. Chem.* **1983**, *253*, 17–30.

(48) Benn, R.; Büch, H. M.; Reinhardt, R.-D. *Magn. Reson. Chem.* **1985**, *23*, 559–564.

(49) Hao, N.; McGlinchey, M. J.; Sayer, B. G.; Schrobilgen, G. J. *J. Magn. Reson.* **1982**, *46*, 158–162.

(50) Xu, Q.; Heaton, B. T.; Jacob, C.; Mogi, K.; Ichihashi, Y.; Souma, Y.; Kanamori, K.; Eguchi, T. *J. Am. Chem. Soc.* **2000**, *122*, 6862–6870.

(51) Maliarik, M.; Glaser, J.; Tóth, I. *Inorg. Chem.* **1998**, *37*, 5452–5459.

(52) Paonessa, R. S.; Trogler, W. C. *J. Am. Chem. Soc.* **1982**, *104*, 1138–1140.

(53) Goggin, P. L.; Goodfellow, R. J.; Haddock, S. R.; Knight, J. R.; Reed, F. J. S.; Taylor, B. F. *J. Chem. Soc., Dalton Trans.* **1974**, 523–533.

(54) Rochon, F. D.; Bubulei, V. *Inorg. Chim. Acta* **2004**, *357*, 2218–2230.

(55) Musco, A.; Pontellini, R.; Grassi, M.; Sironi, A.; Meille, S. V.; Rüegger, H.; Ammann, C.; Pregosin, P. S. *Organometallics* **1988**, *7*, 2130–2137.

(56) Mann, B. E. *J. Chem. Soc., Dalton Trans.* **1973**, 2012–2015.

(57) Keiter, R. L.; Verkade, J. G. *Inorg. Chem.* **1969**, *8*, 2115–2120.

(58) Fischer, E. O.; Knauss, L.; Keiter, R. L.; Verkade, J. G. *J. Organomet. Chem.* **1972**, *37*, C7−C10.

(59) Caldarelli, S.; Catalano, D.; Di Bari, L.; Pasquali, M.; Veracini, C. A. *Gazz. Chim. Ital.* **1990**, *120*, 211–213.

(60) Banck, J.; Schwenk, Z. *Z. Phys. B* **1975**, *20*, 75–80.

(61) Young, C. G.; Kober, E.; Enemark, J. H. *Polyhedron* **1987**, *6*, 255–259.

(62) Hawk, R. M.; Sharp, R. R. *J. Chem. Phys.* **1974**, *60*, 1009–1017.

(63) McFarlane, W. *Mol. Phys.* **1967**, *13*, 587–588.

(64) Schumann, C.; Dreeskamp, H. *J. Magn. Reson.* **1970**, *3*, 204–217.

(65) Clarck, R. J. H.; Davles, A. G.; Puddephatt, R. J.; McFarlane, W. *J. Am. Chem. Soc.* **1969**, *91*, 1334–1339.

(66) Bryce, D. L.; Wasylishen, R. E. *J. Am. Chem. Soc.* **2000**, *122*, 3197–3205.

(67) Zechmann, C. A.; Boyle, T. J.; Pedrotty, D. M.; Lang, D. P.; Scott, B. L. *Inorg. Chem.* **2001**, *40*, 2177–2184.

(68) Berg, K. E.; Blixt, J.; Glaser, J. *Inorg. Chem.* **1996**, *35*, 7074–7081.

(69) Huber, K.; Herzberg, G. Constants of Diatomic Molecules. In *NIST Chemistry WebBook, NIST Standard Reference Database Number 69*; Mallard, W. G., Linstrom, P. J., Eds.; National Institute of Standards and Technology: Gaithersburg MD, 2005; data prepared by J. W. Gallagher and R. D. Johnson, III. URL: http://webbook.nist.gov.

(70) Gillespie, R. J.; Granger, P.; Morgan, K. R.; Schrobilgen, G. J. *Inorg. Chem.* **1984**, *23*, 887–891.

(71) Malleier, R.; Kopacka, H.; Schuh, W.; Wurst, K.; Peringer, P. *Chem. Commun.* **2001**, 51–52.

(72) Autschbach, J.; Igna, C. D.; Ziegler, T. *J. Am. Chem. Soc.* **2003**, *125*, 4937–4942.

(73) Autschbach, J. *Theor. Chem. Acc.* **2004**, *112*, 52–57.

(74) Khandogin, J.; Ziegler, T. *Spectrochim. Acta* **1999**, *A 55*, 607–624.

(75) Moss, R. E.; Trivedi, H. P. *Mol. Phys.* **1979**, *38*, 1611–1619.

(76) Morrison, J. D.; Moss, R. E. *Mol. Phys.* **1980**, *41*, 491–507.

(77) Schwartz, C. *Ann. Phys.* **1959**, *2*, 156–169.

(78) There are classes of problems where low-order perturbation theory with variationally unstable operators yields well-defined results, although higher order perturbation theory may yield divergent terms. For examples involving operators with δ-function terms see refs 75−77. In such a situation finite-field differentiations can be difficult to keep under control, numerically.

(79) Calculated as $\mathrm{MD} = \mathrm{median}_i(|X_i - \mathrm{median}_j(X_j)|)$.

CT900535D